DESIGN AND RESULTS OF AN EXPERIMENT WITH THE GOAL OF GATHERING DATA ON THE MOTION OF A NON-RIGID BODY IN MICROGRAVITY

M. Blazejczyk, K. Maraj, K. Switek, and K. Synowiec

AGH University of Science and Technology in Cracow, Poland

ABSTRACT

A new approach to examining the motion of uncooperative objects is presented. The design of an experiment whose objective is to collect the data required for the evaluation of a motion prediction algorithm is described here, with an assumption that the uncooperative satellites may have variable mass distribution due to some sloshing fuel inside or flexible, oscillating parts such as solar panels. The data is going to be collected during an experimental campaign in ZARM Drop Tower as a part of the Drop Your Thesis 2020 programme organized by ESA Education Office. This facility provides a stable and precise(10-6m/s2) microgravity environment for about 9 seconds. The experimental campaign is taking place in March 2021.

During the experiment, the motion of two free-floating spheres will be recorded with six high-speed cameras. The recordings are fed to a specially designed vision system, which extracts the position and orientation of each sphere based on visual markers, uniformly distributed on their surfaces. The markers determine the axes of the sphere's body reference frame. The assumption of non-constant mass distribution is realized by a mass-spring system inside the sphere. The displacement of a mass is measured with a distance sensor. This data combined with the position of the sphere and prior knowledge of the geometric-mass parameters allows computing the instantaneous center of mass, principal axes, and inertia tensor of the system. The spherical shape of the object minimizes the probability of collision with the greatest volume available. Choice of the shape of the object is a trade-off between the space available inside and the likelihood of a collision with the capsule. Also, a spherical shape minimizes the effect of aerodynamic drag on its motion. The spheres are 3D printed in SLA technology, which enables fast prototyping and high precision. They are released by a mechanism based on a screw-nut connection. The spheres are wound up on a screw, which is mounted on a BLDC motor. The process of releasing is done by firstly spinning up the motor about the direction of the thread, then stopping and spinning up the screw in the opposite direction, forcing the sphere to unscrew.

The team will present preliminary outcomes of processed experimental data such as real trajectories from the experiment, as well as results of the tests conducted prior to the experimental campaign that demonstrate the performance and eligibility for the experiment of developed subsystems.

Keywords: Space Debris; On-Orbit Servicing; motion prediction; variable mass distribution.

1. INTRODUCTION

The population of Space Debris experienced two significant peaks. The first one, in 2007 was caused by fragmentation of *Feng Yun 1C* satellite [1], and the second one, in 2009 when two satellites: *Iridium 33* and *Cosmos 2251* collided [2]. With each collision, the likelihood of next collisions drastically increase. In [3] Donald Kessler noticed, that consecutive collisions between artificial satellites can lead to cascade increase of the number of such events, which was later called *The Kessler Syndrome* [3]. Many ideas originated on how to mitigate this problem. Space agencies and the commercial market analyzed many different concepts on how to slow down the growth of the space junk. One can find an up-to-date review of active debris removal methods in [4]. The idea of capturing the uncooperative satellite with a satellite equipped with a robotic arm has the advantage of the possibility to dock to the client satellite and to rectitude its mission-functions.

Space agencies conducted demonetisation missions of proximity operations, such as ROTEX [5], ROGER [6], Orbital Express [7]. The European Space Agency's mission: e.Deorbit [8] aimed at capturing and removing from the orbit a large malfunctioned satellites. The North American Space Agency designed the SPHERES test bed, which consists of three experimental satellites that were transported to the International Space Station in 2006 [9]. The goal of this program was to allow researchers to test guidance, navigation and control algorithms in microgravity.

The Black Spheres team's aim was to observe a motion of bodies with non-constant mass distribution. The changing mass distribution imitates sloshing propellant and moving parts inside a malfunctioned satellites. Such feature influences the dynamics of an uncooperative satellites. The main goal of the project is to develop and experimentally evaluate a motion anticipation method for such objects.

There are several different methods of simulating microgravity on Earth i.a. parabolic flights, sounding rockets, and drop towers. The most popular method is the parabolic flight, which provides relatively long duration of microgravity of about 22 seconds [10]. However, the low microgravity level fluctuates between $-2*10^{-2}$g and $2*10^{-2}$g during the flight. Typically, drop towers provide from 2 up to 5 seconds of microgravity [11], depending on their height. A unique facility in Bremen provides up to 9.7 seconds of microgravity by utilizing a catapult system. The capsule in which the experiment is conducted is catapulted from the bottom of a 145 meters high tower, instead of being being dropped from its top. Significant advantage of the drop tower is the low level of acceleration disturbances. The accelerations acting on the experiment in the ZARM drop towers are lower then 10^{-6} g. Even though the duration of the experiment is an important factor, the accuracy of the microgravity is the critical one. Therefore, the drop tower was used for the Black Spheres experiments.

2. PROJECT DESCRIPTION

The goal of the project is to develop and validate an algorithm that will identify parameters, such as moment of inertia, instantaneous center-of-mass and principal axes of the uncooperative satellites, and predict their motion. The experiment was designed to produce data that will allow validation of such method by obtaining recordings of free-floating, rotating objects with non-constant mass distribution.

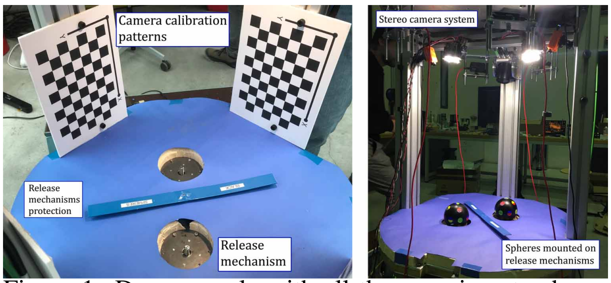

Figure 1: Drop capsule with all the experiment subsystems

The experimental set-up consisted of 3 main subsystems: Vision System, Release Mechanisms and Experimental Objects. The Experimental Objects are spheres rotated and released to move freely inside the capsule in microgravity. The experiment setup is shown on figure 1.

Since the duration of the experiment is very short compared to the duration of an on-orbit inspection phase, sensors should have a high sampling frequency. For these reasons, high-speed cameras were selected by the team. Vision System is a set of algorithms that process recordings from the experiment and approximate the motion of the spheres. It collects data from cameras mounted inside the capsule. Then, it analyzes the video footage, recognizes visual markers, and estimates spheres' position and orientation. In case of the malfunction of either the vision system or the data storage unit, the data from experiments would be lost. This possibility led the team to place redundant inertial sensors inside the spheres.

The spheres were released by a unique mechanism based on a screw-nut connection. Since the experiment was designed for a catapult capsule, which provides a very limited space for the equipment, the whole set-up had to be contained inside a cylinder of 60 centimeters in diameter and 55 centimeters in height. Due to this limitation, there were only two spheres released in each experiment. Avoiding collisions between the spheres and the capsule required high accuracy of the sphere's initial angular rate and vertical velocity. Due to the fact that the capsule is catapulted to an altitude of 120 meters, the experiment has to withhold accelerations of 30g just before the experiment, and deceleration up to 60g when landing.

3. EXPERIMENTAL OBJECTS

For successful observation of non-rigid body dynamics, a well-thought through design of the experimental object is crucial. The requirement of the object's non-rigidity complexified the design, yet it had to be kept simple enough to accommodate rapid prototyping, testing and analysis. The experimental object also had to collect telemetry data such as angular rate and acceleration, for the analysis of its trajectory.

3.1. Design

The object under observation consists of three separable parts: upper hemisphere, lower hemisphere, and guideline. Lower and upper hemispheres were 3D printed using SLA technology. On the surface of each sphere, there were 17 visual markers for their body frame determination via the vision system. The connection with the release mechanism was realized by a nut, fixed to the lower part of a sphere. It was made out of a special *iglidur* plastic - which is characterised by low static and viscous friction coefficients. The outer diameter of the sphere was 88 mm and the inner was 80 milimeters. The interior of the sphere was designed in two variants: guideline with a mass-spring system and with pendulum on a miniature servo.

3.2. Guideline - mass-spring system

The guideline is a rail connected to a 3D printed stand, on which a cart with weight (later called mass) slides. The mass is connected by a spring to the rest of the sphere, and the rail constraints it to move along one axis. The mass weighed around 0.060 kilograms. The whole sphere weighs 0.215 kilograms and the spring has a stiffness coefficient of approximately 90 N/m and a neutral length of 21 millimeters. The displacement of the mass of the spring was measured using the ToF distance sensor. An IMU was placed inside the sphere to measure accelerations and angular velocities of the sphere. All the data was stored on an SD card interfaced with Arduino Nano board. The electronics were powered by a Li-Po battery placed inside the sphere. During the last two experiments, three of the spheres had additional servos to move the mass away from the equilibrium point, introducing additional disturbance. The servo was triggered via Bluetooth after the sphere was released after a certain time. This version of the guideline is presented in figure 2.

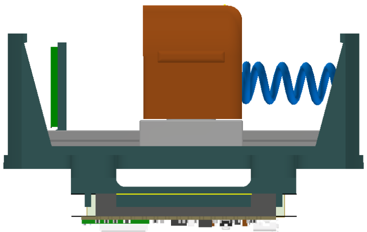

Figure 2: Spring-mass system guideline

3.3. Guideline - pendulum on servo

The second version of the guideline - a pendulum swung by a miniature servo (Power HD-1900A) to which pendulum with a weight of 0.046 kg was connected. The whole sphere weighs around 0.223 kg. A servomechanism was programmed to imitate a motion along a sine wave with a frequency of around 0.33 Hz and an amplitude of 60 degrees. The electronics and the servo were powered by a Li-Po battery placed inside the sphere. Servo was triggered to start moving via Bluetooth after the sphere was released. However, because of the misalignment between the system's centre of mass and the axis of rotation the initial horizontal velocity was too high. Therefore, it was used in only one of the experiments. This version of the guideline is presented in figure 3.

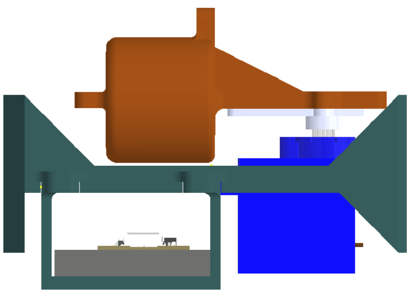

Figure 3: Pendulum servo system guideline

3.4. Analysis

For the sphere with a mass-spring system, the displacement of the centre of mass about the geometrical centre of the sphere was calculated. It was done for three cases:

1. Sphere without amass-spring system.
2. Sphere with a mass-spring system, where spring was in the natural state.
3. Sphere with a mass-spring system, where spring was compressed by ten millimeters.

The calculations were done in the Autodesk Inventor software. In this case, the reference frame was chosen in such a way that the Y-axis was pointing in the direction of the green marker or in other words parallel to the guideline, to the side with the distance sensor. The X-axis was pointing at the red marker, perpendicular to the guideline. The Z-axis was pointing at the nut. The axes are presented in figure 4, and computed values of displacement are present in table 1.

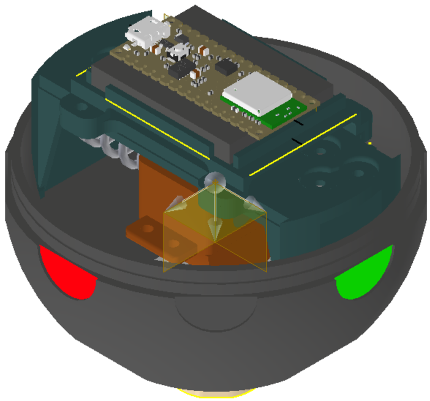

Figure 4: Coordinates inside the sphere

Table 1: Displacement of the center of mass.

Variant	x (mm)	y (mm)	z (mm)
No spring:	0.028	0.119	-0.673
Spring(natural):	0.017	-0.713	1,596
Spring(natural - 10mm):	0.017	-3,493	1,596

The moments of inertia were also computed in Autodesk Inventor method software using the inverted integral. The inertia matrix was computed for three cases:

1. Sphere without a mass-spring system (I_{COM_1}).

2. Sphere with a mass-spring but spring in the natural length (I_{COM_2}).
3. Sphere with a mass-spring but spring is compressed by ten millimeters (I_{COM_3}).

$$I = \begin{pmatrix} I_{xx} & I_{xy} & I_{xz} \\ I_{yx} & I_{yy} & I_{yz} \\ I_{zx} & I_{zy} & I_{zz} \end{pmatrix} \tag{1}$$

$$I_{COM_1} = \begin{pmatrix} 165.706 & 0.157 & 0.276 \\ 0.157 & 155.032 & 0.196 \\ 0.276 & 0.196 & 140.061 \end{pmatrix} kg \cdot mm^2 \tag{2}$$

$$I_{COM_2} = \begin{pmatrix} 174.108 & 0.201 & 0.279 \\ 0.201 & 163.163 & 1.097 \\ 0.279 & 1.097 & 144.014 \end{pmatrix} kg \cdot mm^2 \tag{3}$$

$$I_{COM_3} = \begin{pmatrix} 180.992 & 0.279 & 0.216 \\ 0.279 & 150.897 & 4.611 \\ 0.216 & 4.611 & 163.163 \end{pmatrix} kg \cdot mm^2 \tag{4}$$

For the purpose of later calculations, the sphere was weighed. The results are presented in table 2.

Table 2: Mass of the sphere.

Variant	Mass (kg)
Without mass-spring system:	0.155
With mass-spring system:	0.215

The tensor of inertia was translated to the geometrical centre of the sphere with parallel axis theorem. It will be used in the future to compare its value with estimation algorithm results.

$$I = I_{COM} + \begin{pmatrix} M(y^2+z^2) & -Mxy & -Mxz \\ -Myx & M(x^2+z^2) & -Myz \\ -Mzx & -Mzy & M(x^2+y^2) \end{pmatrix} \tag{5}$$

Translated tensor of the inertia (Eq. 6, 7, 8):

$$I_1 = \begin{pmatrix} 165.778 & 0.156 & 0.279 \\ 0.156 & 155.102 & 0.208 \\ 0.279 & 0.208 & 140.063 \end{pmatrix} kg \cdot mm^2 \tag{6}$$

$$I_2 = \begin{pmatrix} 174.765 & 0.203 & 0.273 \\ 0.203 & 163.710 & 1.341 \\ 0.273 & 1.341 & 144.123 \end{pmatrix} kg \cdot mm^2 \tag{7}$$

$$I_3 = \begin{pmatrix} 184.162 & 0.291 & 0.210 \\ 0.291 & 151.444 & 5.810 \\ 0.210 & 5.361 & 165.786 \end{pmatrix} kg \cdot mm^2 \tag{8}$$

Where:

- I_{COM} - the tensor of inertia along the axes passing through the centre of mass.
- x, y, z - distances between axes.
- M is a mass of the sphere.

4. RELEASE MECHANISM

During the experiment, two of described Spheres were moving in the capsule with a certain linear and rotational speed. The Release Mechanism was the subsystem responsible for releasing the Spheres with prespecified initial angular and linear velocity. There were many trade-offs to consider when designing the mechanism. The angular velocity is limited by the sampling rate of the vision system, but on the other hand, it should be as high as possible so that the effect of the imbalance of the moving mass is visible. Linear speed is constrained by the size of the experimental space and also affected by the angular rate. In addition, the sphere should be released with the required motion properties as quickly as possible - to make full use of approximately 9 seconds of microgravity during the experiment.

4.1. Screw and nut (Release Mechanism model)

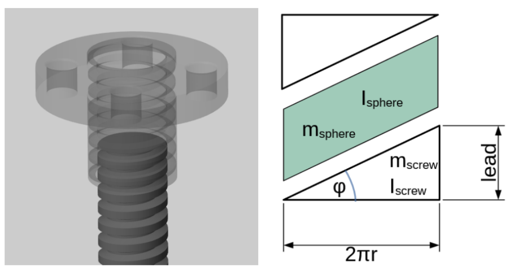

Figure 5: Isometric view of the lead screw and nut (on the left), simplified scheme of mechanism - inclined plane (on the right).

The screw and nut machine with the right actuation provides a helix-shape motion of the nut. The simplicity of such a solution makes that choice the base for the Release Mechanism. In the lead screws the rotation of a nut is constrained by linear couplings. In that solution, the nut, as an integral part of the sphere is a part that shall rotate and translate.

That concept can be represented as an inclined plane, where torque translates into force and angular velocity becomes translational velocity (Fig. 5). That one dimensional physical model is sufficient enough for basic calculations. If α is a difference between the nut's angular rate (θ) and the screw's angular rate (ϕ):

$$\alpha = \theta - \phi \tag{9}$$

Then the relationship between the vertical displacement (x) of the sphere and α for observer in the capsule becomes:

$$x = \frac{\alpha L}{2\pi} \tag{10}$$

The proportionality factor L is the pitch height of the screw (lead). After differentiation:

$$\dot{x} = \frac{\dot{\alpha} L}{2\pi} \tag{11}$$

Where:

- $\dot{\alpha}$ - angular velocity difference ($\dot{\theta} - \dot{\phi}$),
- $\dot{x}$ - vertical velocity of the nut,

The kinetic energy is expressed as follows:

$$T = \frac{I_{screw}\dot{\phi}^2}{2} + \frac{I_{sphere}\dot{\theta}^2}{2} + \frac{m_{sphere}\dot{x}^2}{2} \tag{12}$$

In generalized coordinates θ, ϕ :

$$T = \frac{I_{screw}\dot{\phi}^2}{2} + \frac{I_{sphere}\dot{\theta}^2}{2} + \frac{m_{sphere}(\frac{(\dot{\theta}-\dot{\phi})L}{2\pi})^2}{2} = \\ = \frac{I_{screw}\dot{\phi}^2}{2} + \frac{I_{sphere}\dot{\theta}^2}{2} + \frac{m_{sphere}(\dot{\theta}-\dot{\phi})^2 L^2}{8\pi^2} \tag{13}$$

Where:

- I_{screw} - Inertia of the screw about main axis of rotation,
- I_{sphere} - Inertia of the sphere about main axis of rotation

The potential energy:

$$V = m_{sphere} g(t) x \tag{14}$$

In generalized coordinates θ, ϕ :

$$V = m_{sphere} g(t) \frac{(\theta - \phi)L}{2\pi} \tag{15}$$

In fact the g "constant" changes during the experiment, starting from 1 g through a momentary peak to 30 g, microgravity and peak to 50 g. The Lagrangian function is determined by the kinetic and potential energies of the system:

$$L(\theta, \phi, \dot{\theta}, \dot{\phi}) = T - V \tag{16}$$

The equations of motion are expressed through the Lagrangian formalism in the following form:

$$\frac{d}{dt}(\frac{\partial L}{\partial \dot{q_k}}) - (\frac{\partial L}{\partial q_k}) = \tau_k \tag{17}$$

where τ_k represents the generalized torque in the q_k direction, $k = 1, ..., n$. In ϕ direction there is τ_{act} torque from rotating actuator and $\tau_{friction}(\dot{\theta} - \dot{\phi}, F_{load})$ torque which is produced by friction between nut and screw. The friction torque depends on relative velocity and on load, which vary in different stages of the experiment.

$$I_{screw}\ddot{\phi} - m_{sphere}\frac{L^2(\dot{\theta} - \dot{\phi})\ddot{\phi}}{4\pi^2} - m_{sphere} g(t)\frac{\phi L}{2\pi} = \\ = \tau_{act} \tag{18}$$

$$I_{sphere}\ddot{\theta} + m_{sphere}\frac{L^2(\dot{\theta} - \dot{\phi})\ddot{\theta}}{4\pi^2} + m_{sphere} g(t)\frac{\theta L}{2\pi} = \\ = \tau_{act} - \tau_{friction}(\dot{\theta} - \dot{\phi}, F_{load}) \tag{19}$$

The Stribeck/Coulomb/Viscous model of friction was assumed (Fig. 6) - sliding materials of screw and nut against each other is a source of friction and depends mainly on the relative velocity. [12].

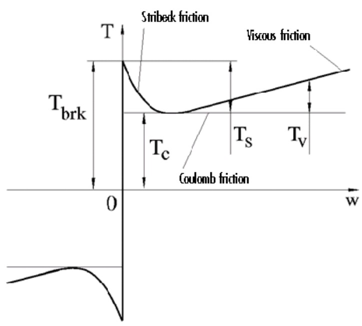

Figure 6: Friction and relative velocity dependency.

4.2. Releasing procedure

The linear velocity of the nut, and consequently the sphere, depends on the difference between the angular

Table 3: Experiment stages

Stage	Time after catapult	g level	Description
1	-7s	1g	The screw with the sphere wounded on it accelerates (reaching target angular velocity).
2	0s	Up to 30g	The sphere is slightly rebounded due to high overload.
3	300 ms	0g	The screw rotation is immediately reversed and the Sphere unscrews due to its inertia.
4	500-700ms	0g	The Sphere is released and rotates freely in the capsule under microgravity conditions.
5	1.6s	0g	Second release trial.
6	3.55	0g	Third release trial.
7	5.2	0g	Motors stop.

velocities of the screw and the nut (Eq. 11). Additionally, the inertia of the screw is negligible compared to the inertia of the sphere in the dynamics equations (Eq. 18, 19). Hence, the idea of the following sphere's release procedure:

1. Spin up the screw with the sphere wounded on it to the target angular velocity.
2. After microgravity occurs, change the angular velocity of the screw.

The sphere will keep spinning in the same direction, causing the angular velocity difference between the sphere and the screw. The sphere leaves the screw. The vertical velocity of the sphere is directly proportional to the difference in the angular velocity of the screw and the sphere as it leaves the mechanism. Such a trajectory of motion is easy to optimize for required parameters:

1. The linear speed of the sphere is controlled by adjusting the difference between screw angular velocity in the first stage and during the releasing (stage 3).
2. The angular velocity of the sphere shall be controlled by adjusting the set screw angular velocity before the releasing (stage 1).
3. If the sphere does not leave the screw, change the initial position of the sphere (choose plug with different high).

It is important to consider the angular velocity drop due to the frictional torques between sliding bodies in the above conclusions. The velocity loss increases exponentially as the difference in velocity decreases, but there is a lot of uncertainty due to friction and backlash. The above stages, taking into account the gravity conditions during the experiment, are presented at the table 4. Simplified scheme of the procedure are shown at the figure 7.

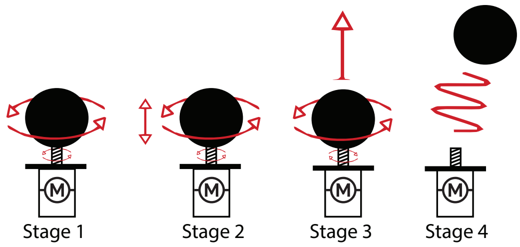

Figure 7: Experiment stages.

In the first stage of the experiment, the mass on the spring moved to the wall of the sphere due to centrifugal force. The higher the rotational speed, the greater the mass shift. That effect is desirable - the effect of variable mass distribution is more visible with higher initial mass displacement. But on the other hand the sphere's imbalance influences friction coefficient and initial XY linear velocity.

4.3. Release Mechanism design

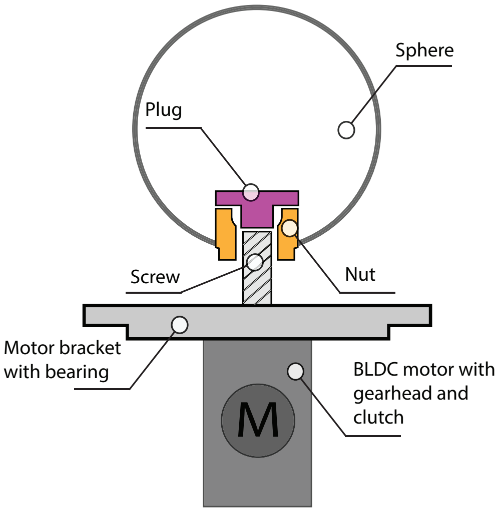

Figure 8: Simplified scheme of Release Mechanism components

With such an idea, the selection of the right actuator and screw with the right pitch and low friction coefficient was crucial. The Faulhaber BLDC motor with a planetary gear was responsible for the screw actuation. It had an sufficient range of rotational rates (from about -5500 rpm to 5500 rpm) and provided a high acceleration torque τ_{act} - very important to achieve desired motion trajectory. The choice of the screw pitch (L) determined the space of possible vertical velocities. Simulations for different friction coefficients proved that pitch at high $12mm$ was a right choice. To lower the friction coefficient a screw-nut connection with an unusual profile was used - *dryspin®* from Igus company. Faulhaber Motion Controller was responsible for controlling the motor. This controller has a functionality of defining the motion profiles - mainly the acceleration rate and deceleration rate. That allows to generate complex profiles. The Sphere was secured against axial displacement (in proper direction) through the use of an 3D-printed plug. The scheme of the system is shown on figure 8. A several plugs with different heights were printed so that it was possible to change the initial position of the sphere between experiments.

4.4. Placement determination

A multibody model of the system was built to take into account inbalance effect of the moving mass. Figure 9 shows possible trajectories for the model. In the simulation, a constant difference between the speed in the first stage and the third stage was assumed.

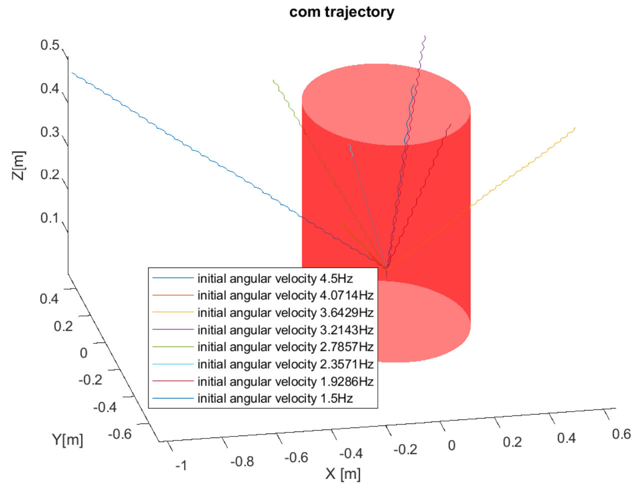

Figure 9: Possible trajectories of the Sphere for different angular velocities in the first stage (red roller with allowable space)

Taking into account simulations results, 2 Release Mechanisms were placed at equal intervals from the capsule border. In the picture 10 the red and yellow sections are equal in length to 20 cm.

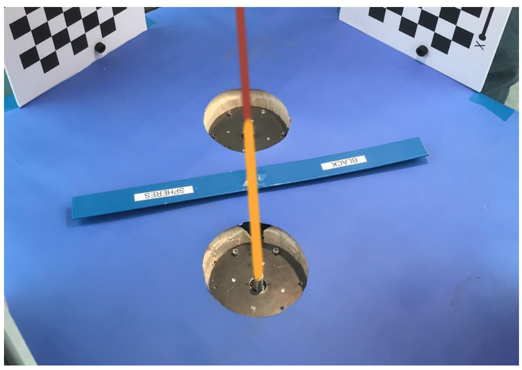

Figure 10: Release Mechanisms placement

4.5. Trajectory and parameters

Step response of the motors was fast enough to perform releasing procedure described in section 4.2. However, assuming high uncertainty related to friction, the procedure was extended by 2 additional release attempts with higher velocity difference to decrease velocity drop. Example trajectory is shown in Figure 11.

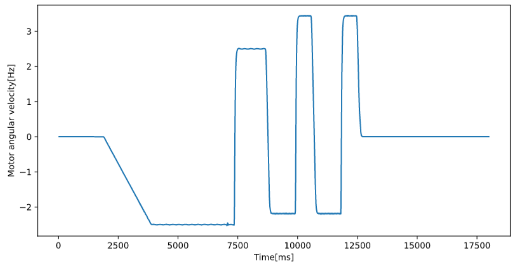

Figure 11: Release Mechanisms example trajectory

The motors started spinning up 7 seconds before the each catapult. Such a short time was important to maintain the repeatability of the final position of the motors between experiments. Moreover, the dynamics of the motors was slightly different, results in a different end position (with the same parameters - Fig. 12). 7 seconds was enough to neglect that effect in trajectory planning.

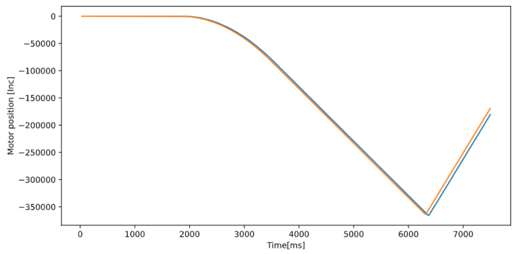

Figure 12: Position difference in time for two motors (orange motor 1, blue motor 2)

The angular velocity of the screw in the first and third stages (Table 4, Figure 17) was adjusted between experiments. This was necessary due to the slightly different friction of the screw-nut connection between the release mechanisms, resulting in different velocity drop characteristics.

5. VISION SYSTEM

The main objective of a vision system in the experiment was to collect and process video footage from all the experiments. Computer vision algorithms allow detection of experimental spheres and approximation of their position and orientation relative to the capsule. In order to achieve three-dimensional position approximation by stereo vision techniques of an object at least two cameras are required. In this way an information about depth is obtained and the trajectory of a sphere can be reconstructed. The two key factors that affect the quality of a video footage are resolution and frame rate. The team decided to use 6 cameras in order to have a system where both spheres are seen during the whole experiment. There were four GoPro Hero 8 Black cameras allowing to record with Full HD resolution and a rate of 240 frames per second and two RunCam2 cameras recording with the same resolution and 120 frames per second. The cameras were placed on the upper part of the capsule around its perimeter. With their wide field of view of about 130 degrees they allowed to record the whole trajectory of experimental spheres during the whole 9 seconds of microgravity. The configuration is shown in figure 13.

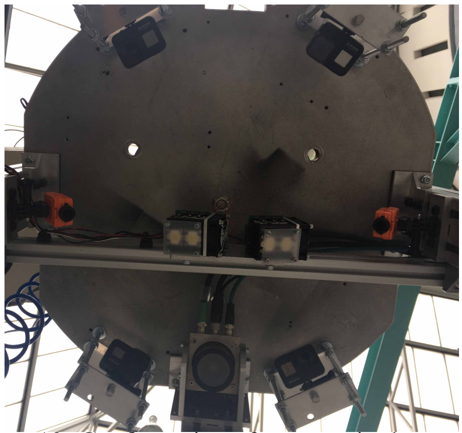

Figure 13: Configuration of cameras in the capsule

Sphere detection was based on circular Hough transform. The algorithm detected two spheres on the footages from the capsule, distinguished between them and followed their trajectories. Each sphere was covered with color markers that determined its body reference frame. To maintain the invariance of brightness, an HSV colorspace was used, as it has separate channels for the color, its saturation and brightness (value). Later, a sequence of morphological operations and filters was applied in order to obtain a binary image showing the exact position of a sphere on an image. Criteria, such as eccentricity and area of a detected object ensured that it is of a circular shape. Later the markers are detected inside the area of a sphere. A photo taken from one of the cameras and after image processing showing the sphere and detected markers on its surface is presented in figure 14.

Figure 14: Detected spheres and markers on their surfaces. In the background there are 3 calibration patterns

Sphere's position estimation was based on triangulation method. Firstly, all the cameras are calibrated in pairs in stereo configurations. An example of a calibration pattern seen by cameras is shown in figure 15. The quality of calibration is determined by measuring the distance between the point on one image and its reprojection from the second image. The output of such a procedure are intrinsic parameters for both cameras, their relative pose in terms of rotation matrix and a translation vector. Also, a transformation from the camera to the calibration plate's reference frame is obtained which allows to transform from the camera to the capsule's reference frame. Now, with the calibrated camera configuration it is possible to reconstruct the 3D motion of an object by analysing its positions in recordings from both cameras. The locations of spheres in every frame were extracted from both videos and fed to the triangulation algorithm. This information, along with a matrix containing the pose of one camera relative to another (known as *fundamental matrix* [13]) allows to compute the 3D positions of a sphere. Position calculated in such a way is represented in camera reference frame. Later the position and orientation are transformed to the capsule reference frame which is determined by the centre of capsule's bottom plate with Z axis pointing upwards.

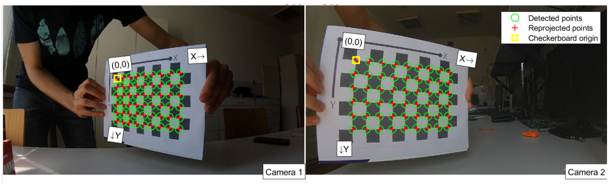

Figure 15: Camera calibration patterns

The vision system detected oscillations of both rotating spheres related to the uneven mass distribution. The concept for orientation estimation was based on [14] and [15]. As shown before in this section, two cameras are able to find a geometrical center of a sphere. If the distribution of markers is given and the stereo vision algorithm finds a point on a sphere surface, a vector connecting those two points can be created. This gives an information about orientation of one axis with reference to the capsule, however the system is not fully constrained as it may rotate around this axis (case a). It is shown on figure 16. When a second point is found the system is fully constrained and the estimation of orientation axes is given (case b).

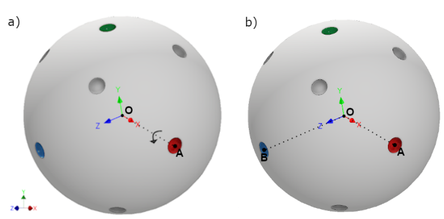

Figure 16: A concept of 3D orientation estimator

Markers on a sphere determine both main orientation axes, such as X+, X-, Y+, Y-, Z+, Z- and their bisectors (XY, XZ, YZ...) - in total 17 markers. When two points on a sphere are found, two orientation axes can be determined directly. The third orientation axis is calculated by taking a cross product of two previously found vectors. A transformation from bisector to the main axis is calculated when required. Having three vectors corresponding to main axes, a rotation matrix can be formed, representing the orientation of a sphere relative to capsule reference frame.

In the Results section the first estimations of sphere trajectories are presented.

6. OUTCOME

6.1. Experimental Campaign

The experimental campaign took place in March 2021 and lasted for two weeks. The first week was intended to integrate the team's and ZARM's devices. This time was also spent on conducting final unit tests and integration tests of the experimental apparatus. In the second week, the experiments were conducted - during five consecutive days, five catapults were done (one per day). The outcome of all catapults was presented in table 4.

6.2. Results

In this chapter the preliminary results from processed experiment data are presented. Firstly, estimations from the vision system are presented. On figure 21 there are trajectories of two spheres from two experiments.

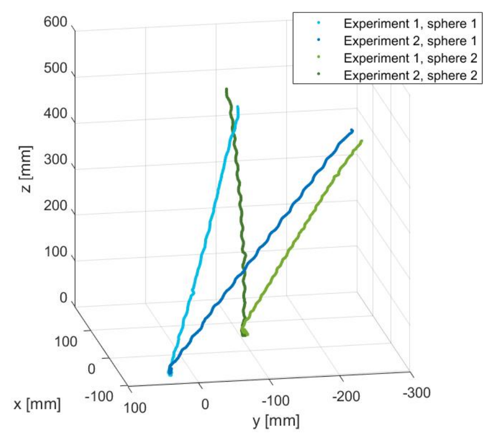

Figure 21: Reconstructed 3D trajectories of spheres

Due to limited height of capsule the velocity in the Z axis along the capsule's height had to be controlled. This way during the whole 9 seconds of microgravity the cameras placed in the upper part of the capsule were able to record the spheres. Positions of spheres in Z axis are shown on figure 22.

Table 4: Summary of the experiments. The outcome of the first and the second release procedures and collision occurrence.

Catapult	Sphere 1	Sphere 2	1st release	2nd release	Collision
1	Mass-spring	Mass-spring	☑	☐	☐
2	Servo pendulum	Servo pendulum	☐	☑	☐
3	Mass-spring	Mass-spring	☑	☐	☑
4	Mass-spring	Mass-spring plus servo	☑	☐	☐
5	Mass-spring plus servo	Mass-spring plus servo	☑	☐	☐

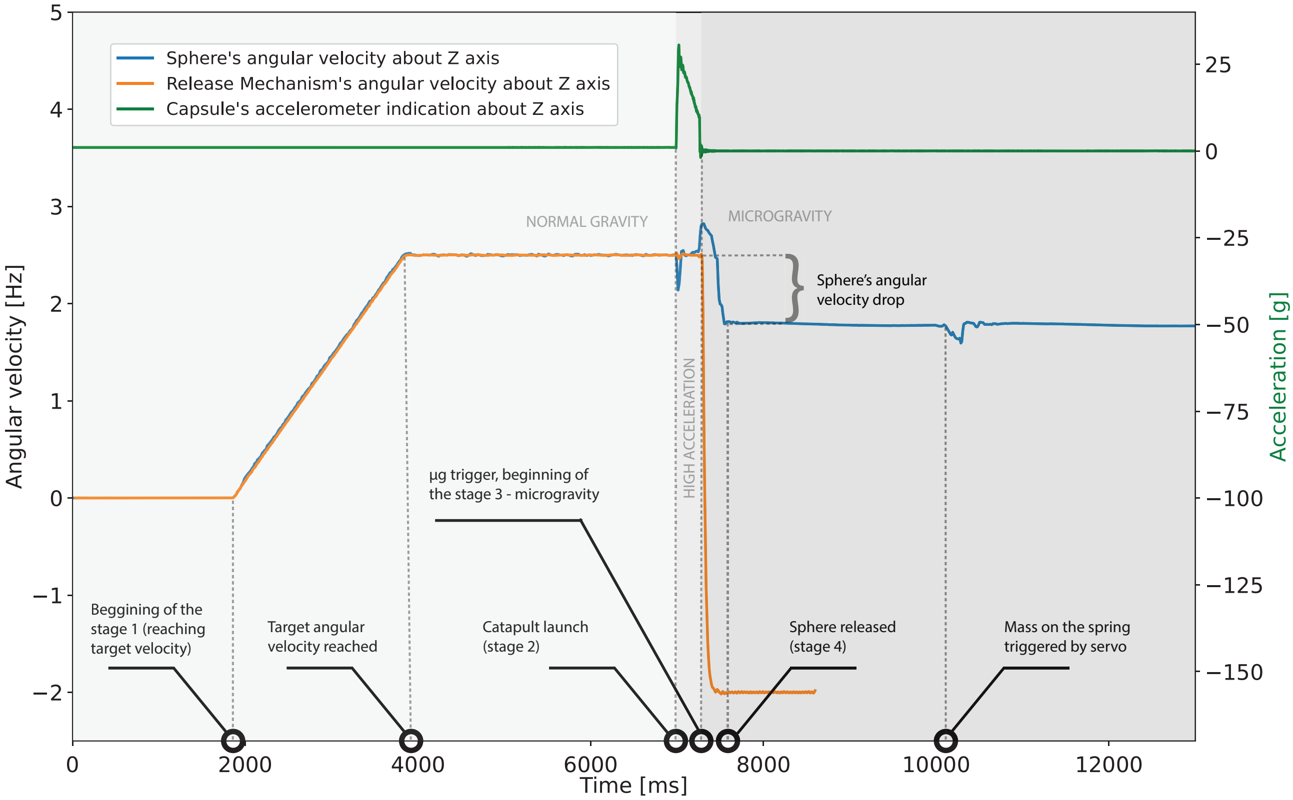

Figure 17: Experiment stages on the example of one of the Spheres in the 5th experiment.

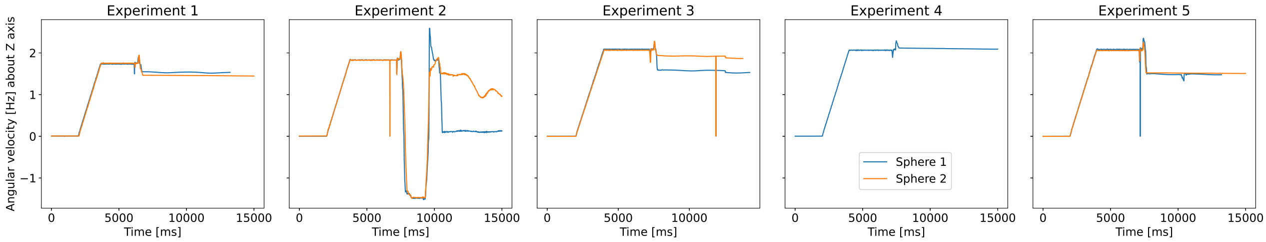

Figure 18: Data from IMU gyroscope in the following experiments.

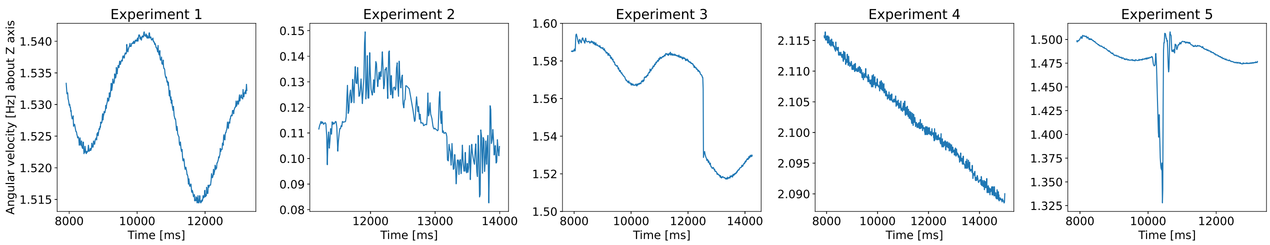

Figure 19: Detailed data for microgravity stage from IMU gyroscope in the following experiments for the first sphere.

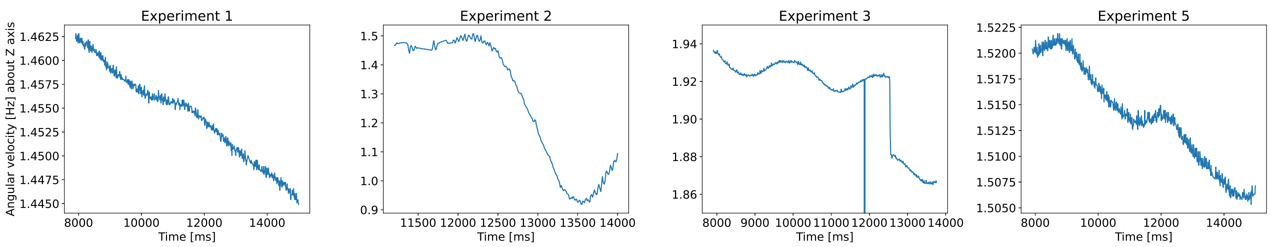

Figure 20: Detailed data for microgravity stage from IMU gyroscope in the following experiments for the second sphere.

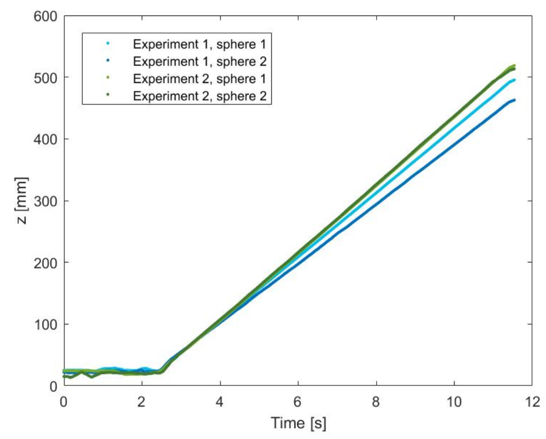

Figure 22: Positions of spheres along Z axis during the experiments

On figure 21 there are visible oscillations of spheres due to uneven and variable mass distribution. They are better noticeable on the XY projection of sphere's trajectory. Such a projection is shown on figure 23.

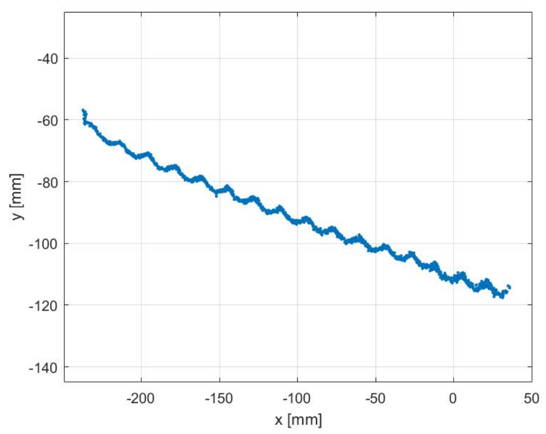

Figure 23: Position of a sphere in XY plane during the drop experiment

7. CONCLUSIONS

The team conducted a successful experimental campaign. The mechanisms designed by the team allowed achieving controlled release of spheres and avoiding collisions with the capsule's hardware. Although the spheres experienced about 50 g during the deceleration phase some of them survived the landing. Each experiment provided plenty of data to analyse - both from the vision system and the sensors inside the spheres. There are noticeable oscillations which will be thoroughly examined to develop a motion prediction algorithm. The universality of the collected data will allow to test and evaluate different estimation methods for objects with non-constant mass distribution. Due to the fact that this is the first team's approach to the problem, there still is a room for improvement. The experiment can be viewed as a proof-of-concept of the team's approach to examining the motion of objects with varying mass distribution and new ideas which could give better results of the position and orientation determination. There is also a necessity to build new test stands to verify the accuracy of such algorithms. Should the results of March campaign be auspicious the team will search for opportunities to continue the research on tracking the uncooperative objects with variable mass distribution and perform more microgravity experiments.

ACKNOWLEDGMENTS

The team would like to thank the coordinators from ESA Academy and experts from ZARM Drop Tower Institute for the guidance and feedback given during the project development, and Paweł Zagórski PhD for giving the inspiration to the team.

REFERENCES

1. H. Kurosaki, T. Yanagisawa, and A. Nakajima, Optical Observation of LEO Debris Caused by Feng Yun 1C. Transactions of The Japan Society for Aeronautical and Space Sciences, Space Technology Japan. 2009
2. A. Tan, T. X. Zhang, M. Dokhanian, Analysis of the iridium 33 and cosmos 2251 collision using velocity perturbation of the fragments. Advances in Aerospace Science and Applications. 3, 13-25, 2013.
3. D.J. Kessler and B.G. Cour-Palais, Collision Frequency of Artificial Satellites: The Creation of a Debris Belt, Journal of Geophysical Research, Vol. 83, No. A6, pp. 2637-2646, June 1, 1978.
4. C. Priyant Mark, Surekha Kamath, Review of Active Space Debris Removal Methods, Space Policy Volume 47,Pages 194-206, 2019.
5. G. Hirzinger and B. Brunner, J. Dietrich, J. Heindl, ROTEX-the first remotely controlled robot in space, 1994 IEEE International Conference o
6. B. Bischof, Roger - Robotic Geostationary Orbit Restorer, 54th International Astronautical Congress of the International Astronautical Federation, the International Academy of Astronautics, and the International Institute of Space Law, 2003.
7. A. Ogilvie, J. Allport, M. Hannah, and J. Lymer, Autonomous satellite servicing using the Orbital Express Demonstration Manipulator System. 9th International Symposium on Artificial Intelligence, Robotics and Automation in Space, Los Angeles, USA, 2008.
8. S. Jaekel, R. Lampariello, W. Rackl, B. Brunner, O. Porges, E. Kraemer, M. Pietras, J. Ratti, R. Biesbroek: Robotic aspects and analyses in the scope of the

e.Deorbit mission Phase B1. 14th Symposium on Advanced Space Technologies in Robotics and Automation, Leiden, The Netherlands, 2017.

9. B.E. Tweddle, A. Saenz-Otero,, and D.W. Miller, The SPHERES VERTIGO Goggles: Vision Based Mapping and Localization onboard the International Space Station, International Symposium on Artificial Intelligence, Robotics and Automation in Space, Turin, Italy, 4-6 September, 2012.
10. V. Pletser,Parabolic Flights, In book: European Users Guide to Low Gravity Platform, Chapter 4, January, 2005
11. T. Könemann, U. Kaczmarczik, A. Gierse, A. Greif, T. Lutz, Concept for a Next-Generation Drop Tower System. Advances in Space Research, 55, 2015
12. B. Armstrong, C.C. de Wit, Friction Modeling and Compensation, The Control Handbook, CRC Press, 1995
13. R. Hartley and A. Zisserman, "Multiple View Geometry in Computer Vision" 2003, pp. 266–267
14. Feng Yu, Zhen He, Bing Qiao and Xiaoting Yu, Stereo-Vision-Based Relative Pose Estimation forthe Rendezvous and Docking of Noncooperative Satellites, 2014.
15. K. Switek, Stereovision based position and orientation estimator of objects inside drop tower capsule, AGH 2020. n Robotics and Automation, pp. 2604-2611 vol.3, San Diego, CA, USA, 1994.